# NOISE REDUCTION IN ULTRASONIC NON-DESTRUCTIVE EVALUATION (NDE) AND IMAGING

Minghui Li [1, a)] and Gordon Hayward [2]

[1]*School of Engineering, University of Glasgow, Glasgow G12 8QQ, United Kingdom*
[2]*Alba Ultrasound, Unit 1, Block 3, Todd Campus, West of Scotland Science Park, Glasgow G20 0XA, United Kingdom*

[a)]Corresponding author: minghui.li@ieee.org

**ABSTRACT –** Reliable and robust defect detection is a challenging yet essential problem in ultrasonic non-destructive evaluation (NDE). The flaw echoes are usually contaminated by high-level time-invariant grain noise originating from the material microstructures. This phenomenon becomes even worse when inspecting coarse-grained materials like austenitic stainless steel, alloy, carbon-reinforced composite and concrete, which however, form some of the most important and commonly used industrial materials. This problem has attracted great attentions from the NDE community and a wide variety of techniques have been investigated to enhance the signal-to-noise ratio (SNR) and flaw detection. In this chapter, the signal processing approaches that exploit the spatial and temporal-spectral characteristics of the flaw echo and noise for enhanced defect detection and noise reduction in ultrasonic NDE are presented. The first category of techniques exploits the spatial diversity created by the transducer array, and utilises spatial filtering to discriminate the flaw echo from the clutter noise. Particularly, minimum variance beamforming seeks to minimize the power of the array output while maintaining a unit gain on the focal point, and weighs the observations with data-dependent apodization. The second category of approaches investigates the time-frequency analysis and statistical properties of flaw echoes and grain noise. In particular, the advanced matched filter is designed to match unknown flaw echoes rather than the transmitted signal, and utilise an optimization paradigm to tweak and search the best filter parameters. Results from simulation studies and experiments on the real industrial samples are presented to evaluate the techniques, and demonstrate their robustness and advantages over the classical methods.

**KEYWORDS –** non-destructive evaluation, ultrasound, matched filtering, adaptive beamforming

## 1. INTRODUCTION

Reliable and robust flaw detection in the presence of grain noise is a challenging yet essential problem in ultrasonic non-destructive evaluation (NDE), which has attracted significant attention from the NDE community in recent decades [1-17]. A variety of coarse-grained materials like alloy and austenitic stainless steel offer attractive properties

like high-temperature strength or excellent resistance to corrosive environment, and thus are widely used to build components like ducting, combustion cans, and transition liners in a range of key industrial sectors such as energy, oil and gas, nuclear, and aerospace. However, those materials composed of coarse-grained structures may pose significant challenges for ultrasonic pulse-echo inspection techniques, because the flaw echoes are usually contaminated by significant grain noise originating from the material microstructures, furthermore, the grain noise is time-invariant, demonstrating similar spectral characteristics, and correlated with the flaw echoes.

A wide variety of techniques have been investigated to suppress grain noise and enhance flaw detection through exploiting the key differences between defect echoes and grain noise. Since the defect (or a legitimate reflector) and grain boundaries often have different sizes, their scattering properties and responses have different spectral characteristics [3]. These differences have motivated temporal-spectral processing techniques given that the excitation signals are usually broadband, such as Weiner filtering [4, 5], split-spectrum processing [6-8], fragment recognition classifier [9], sub-spectrum phase coherence factoring [10], spectral distribution similarity analysis [11], and matched filtering [12, 13]. The defect echo typically has a coherent structure with energy mainly scattered from a single spatial point, while grain noise are spatially distributed throughout the insonified resolution cell. These differences have motivated spatial diversity and processing techniques, such as spatial beamforming [2, 14], coherence factoring [15], and spatially averaged sub-array correlation imaging [16, 17].

This chapter focuses on advanced matched filtering and spatial beamforming techniques for noise reduction in ultrasonic NDE. The signal matching concept has been extensively used in the detection of signals of known form in stationary noise in applications like radar and sonar [18], and more recently in the field of ultrasonic NDE [19, 20]. If the signal waveform and noise statistics are exactly known *a priori*, the matched filter is optimal in terms of the signal-to-noise ratio (SNR) improvement; this is unfortunately not the case in NDE. In this chapter, the matched filter design is investigated and extended into the scenario of inspection of coarse-grained materials. The filter is tuned to match the unknown defect echoes (rather than the transmitted signal) which are approximated by the superposition of multiple transmitted signals with different phase shift, time delay and amplitude gain that simulate reflections from an unknown spatially extended defect. An optimization paradigm is employed to search for the optimal parameters in the filter response in order to maximize the SNR gain over a set of training signals.

In addition to matched filtering, this chapter presents a spatial filtering approach which utilises adaptive beamforming in reception to suppress grain noise and enhance defect echoes, with the assumption that they originate from different spatial locations. Adaptive beamforming applies a delay-weight-and-sum operation to the received signals across the probe aperture, where the adaptive weights are computed from the statistical analysis of the data samples based on the minimum variance theory. The ways of increasing robustness in NDE scenarios are considered.

The chapter is organised as follows. Section 2 presents the data model for the defect and grain echoes in ultrasonic NDE, and discusses the design and implementation of the optimised matched filter. Section 3 formulates the problem of spatial beamforming, presents the minimum variance adaptive beamformer, and discusses the techniques to enhance its robustness in the presence of mismatches or errors like wrong assumptions of acoustic velocity or phase aberrations. Section 4 presents experiments on real industrial samples and simulation studies to evaluate the performances of the adaptive beamformer and the optimised matched filter for noise reduction and defect detection against the classical methods. The chapter is then concluded.

## 2. OPTIMAL MATCHED FILTER DESIGN IN TEMPORAL-SPECTRAL DOMAIN

### 2.1. Data model in ultrasonic NDE

This section describes the ultrasonic data model, which is used for the optimal matched filter design. If there is a single point reflector in a homogeneous and lossless propagation media, the return signal $x(t)$ at the receive (rx) element is equal to the signal $s_0(t)$ transmitted from the transmit (tx) element except for a time delay $t_0$ and scaling factor $A$,

$$x(t) = As_0(t - t_0). \tag{1}$$

The propagation distance from the tx element to the point reflector and back to the rx element can be calculated from the coordinates of the transmit and receive elements and the reflector. And the propagation time, or time delay $t_0$, is determined by dividing the propagation distance by the longitudinal velocity of sound in the media. The amplitude scaling factor $A$ is employed to address the effects of element directivity and beam spread, as well as the effect of the divergence of the waves from the tx element and from the point reflector. The above-mentioned point reflector signal model is straightforward to follow, and has been used in a variety of literature on radar [21, 22], communications [23, 24], and ultrasonic imaging [25] as a standard data model.

However, in most practical ultrasonic NDE applications, the defects cannot be simply represented by single or well isolated point reflectors; instead most defects are spatially extended and distributed with a spatial shape or profile. A straightforward yet reasonable extension to the above data model for a distributed defect is that the defect consists of a number of point-like reflectors, each with given scaling and characteristics due to the effect of element directivity, beam spread, and spatial position that determines the propagation time. For a spatially extended defect, the return signal $x(t)$ received at the rx element is then given by a sum of $J$ delayed and scaled versions of the transmitted signal $s_0(t)$,

$$x(t) = \sum_{i=1}^{J} A_i s_0(t - t_i) + n(t), \tag{2}$$

where $s_0(t)$ is the excitation signal taking into account of the pulser output waveform and the frequency response of the transducer, $J$ is the number of point-like reflectors under consideration for this particular extended defect, $A_i$ and $t_i$ are the amplitude factor and the propagation time delay corresponding to the $i$th point reflector with certain position and reflection characteristics, and $n(t)$ is the additive noise due to the transceiver internal circuit and the environment noise in the media and couplant, which is assumed to be uncorrelated with the defect echoes.

### 2.2. Optimal matched filter design

As shown in the data model (2), the return echo originating from a defect is contaminated by noise, which may consist of the electronic noise in the transmitter/receiver channel circuits, the large amount of reflections from the microstructure grain boundaries within the test sample, the coupling variation between the transducer and the sample, and *etc.*; and the noise could be significant with regard to the signal of interest originating from the defect, and thus results in a poor SNR. Matched filtering is to pass the echoes at the receiver through a filter with a particular response to suppress the noise and enhance the SNR. Assume $x(t)$ is a returned echo from a distributed defect received by a transducer, which is processed by a matched filter with an impulse response $h(t)$, the output signal $y(t)$ is given by

$$y(t) = x(t) * h(t), \tag{3}$$

where * stands for the convolution operation. $x(t)$ is composed of the signal component which is determined by the defect profile and characteristics (shape and reflection factor) as well as the additive noise, as illustrated in the data model (2). Based on the theory of matched filtering, if the filter response $h(t)$ is exactly matched to the echo reflected from the defect (the first part of equation 2), that is

$$h_{opt}(t) = \sum_{i=1}^{J} A_i s_0(t - t_i), \tag{4}$$

the SNR of the filter output $y(t)$ will be maximized. However, the defect echo $s_d(t) = \sum_{i=1}^{J} A_i s_0(t - t_i)$ is unknown, because the number of point reflectors $J$, the delays $t_i$ and the amplitude factors $A_i$ are all unknown, and may differ between samples. The goal of the optimal matched filter design is to tweak the parameters of the filter response $h(t)$ to approximate the unknown defect echo, so that the output SNR is maximized for a set of given training signals.

In mathematics, the above problem of optimal matched filter design can be formulated by the following constrained optimisation equations

$$\max_{A_i, t_i} \mathrm{SNR}\left[y(t)\right] \quad \text{subject to} \quad \begin{aligned} y(t) &= h(t) * x(t) \\ h(t) &= \sum_{i=1}^{K} A_i s_0(t - t_i) \\ x(t) &= \sum_{i=1}^{J} A_i s_0(t - t_i) + n(t) \end{aligned}, \tag{5}$$

where $K$ is the number of point reflectors considered in the approximation to reconstruct the defect echo, which is unknown *a prior* and is a design parameter. The defect echoes could be reconstructed using the actual excitation signals, which are accurate to account for the practical experimental uncertainties [12]; however the process could be troublesome requiring extra efforts and time. In this chapter, we present a more flexible and robust design method which uses simulated excitation signals taking into account of the operation parameters of the transducer and the transmitter-receiver system, to approximate the defect echoes. The experimental results from real industrial samples demonstrate that through the optimization and tuning procedure for the filter parameters, the same good results are obtained from this design routine.

From the problem formulation of optimal matched filter design (5), it demonstrates that the filter response determination consists of two steps: 1) To reconstruct the return echo by using the simulated excitation signal $s_0(t)$ and the design parameters $K$, $A_i$ and $t_i$, $i=1, 2, \ldots, K$; and 2) To tweak the above control parameters until the output SNR is maximized.

In the first step, with a particular set of control parameters $K$, $A_i$ and $t_i$, $i=1, 2, \ldots, K$, the return echoes are reconstructed, which are then employed in the matched filter (5) and the output SNR is calculated. The SNR will be increased or decreased depending on the parameters chosen in the filter. The second step of matched filter design involves tweak the above-mentioned parameters by searching the best values in the problem space, in order to achieve the maximum SNR gain.

Apparently, the search process is not trivial, and the dependence of the cost function $\mathrm{SNR}\left[y(t)\right]$ in equation (5) on the control variables $A_i$ and $t_i$ is supposed to be non-linear, high-dimensional and complicated. A numerical optimization paradigm such as the Genetic Algorithms (GA), Simulated Annealing (SA), or Particle Swarm Optimization (PSO) is in a good position to tackle this problem.

In this chapter, PSO is employed due to its robust and powerful optimisation capability, and simple implementation, as demonstrated in the literature [26]. PSO starts by initializing a population of particles in the search space. The position vector of the $i$th particle takes the form $p_i = \{A_{i1}, t_{i1}, A_{i2}, t_{i2}, \ldots, A_{iK}, t_{iK}\}$. The fitness of particle $p_i$ is computed using the flowchart in Fig. 1. For more details about the update rules and equations of PSO paradigm and evolutionary algorithms, the readers may refer to [26-28] and the references therein.

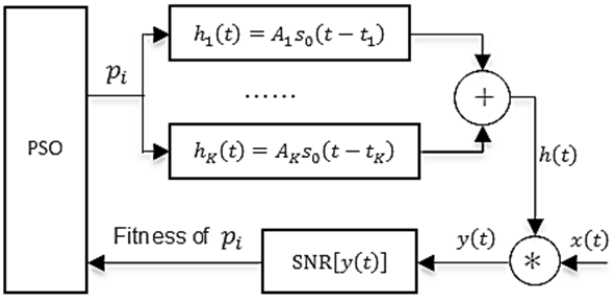


Figure 1. Determination of particle fitness in PSO paradigm.

## 3. SPATIAL FILTERING AND ADAPTIVE BEAMFORMING

### 3.1. Data model and problem formulation

To properly formulate the problem and present the adaptive beamformer, a data model with point reflectors is considered in this section. Assume that there are $J + 1$ point scatters in the insonified region, each reflecting a signal, $s_j(t), j = 0, \ldots, J$. A transducer array of $N$ elements is considered. The time series received at the $n$th element is

$$x_n(t) = \sum_{j=0}^{J} g_{n,j} s_j\left(t - \tau_{n,j}\right) + v_n(t),\ n = 1, \ldots, N, \tag{6}$$

where $g_{n,j}$ represents the amplitude adjustment corresponding to the distance from reflector $j$ to transducer element $n$ and the gain of that element, $\tau_{n,j}$ is the time delay from reflector $j$ to element $n$, and $v_n(t)$ is the noise on channel $n$.

Assume that the transducer array is focused on scatter 0 in reception through delaying each channel by $\tau_{n,0}$, $n = 1, \ldots, N$. Under this assumption, $s_0(t)$ is the desired signal and the other reflectors are sources of interference. The time-delayed signal received at channel $n$ can be described as

$$x_n(t) = g_{n,0} s_0(t) + \sum_{j=1}^{J} g_{n,j} s_j\left(t + \tau_{n,0} - \tau_{n,j}\right) + v_n(t),\ n = 1, \ldots, N, \tag{7}$$

The time-delayed array output vector $\mathbf{x}(t)$ is given by

$$\mathbf{x}(t) = [x_1(t)\ x_2(t)\ \ldots\ldots\ x_N(t)]^T, \tag{8}$$

where $[\bullet]^T$ denotes the transpose operator. The problem to be addressed in this section is to extract the desired signal $s_0(t)$ from the received echoes contaminated by the interference and additive noise using spatial filtering and adaptive beamforming.

3.2. Minimum variance adaptive beamformer

Adaptive spatial filtering and beamforming is achieved by weighting the received echoes with data-dependent apodization, after each channel is appropriately delayed to focus at a point within the insonified media. The flow chart is illustrated in Fig. 2. The output of the beamformer can be described as

$$z(t) = \mathbf{w}(t)^H \mathbf{x}(t), \tag{9}$$

where

$$\mathbf{w}(t) = [w_1(t)\ w_2(t)\ \ldots\ \ldots\ w_N(t)]^T \tag{10}$$

is a weight vector, and $[\bullet]^H$ stands for the operator of conjugate transpose. The minimum variance beamformer (also known as the Capon beamformer) seeks to minimize the power of the beamformed output $z(t)$ while maintaining unit gain on the focal point [29]. This constrained optimization problem can be formulated as

$$\min_{\mathbf{w}(t)} \mathbf{w}(t)^H \mathbf{R}(t)\mathbf{w}(t), \text{ subject to } \mathbf{w}(t)^H \mathbf{a} = 1, \tag{11}$$

where

$$\mathbf{R}(t) = E\left[\mathbf{x}(t)\mathbf{x}(t)^H\right] \tag{12}$$

is the data spatial covariance matrix, and

$$\mathbf{a} = [1\ \ 1\ \ldots\ \ldots\ 1]^T \tag{13}$$

is an $N \times 1$ column vector of ones, because the data have already been delayed to focus on the point of interest. The optimal weight vector is the solution to (11), which is given by

$$\mathbf{w}_{opt}(t) = \frac{\mathbf{R}(t)^{-1}\mathbf{a}}{\mathbf{a}^H \mathbf{R}(t)^{-1}\mathbf{a}}. \tag{14}$$

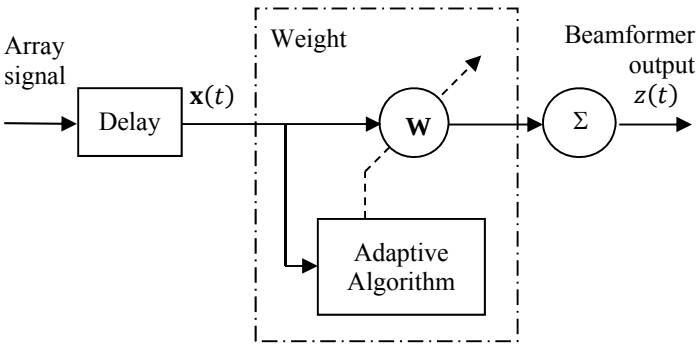


Figure 2. Flowchart of adaptive beamforming.

In practice, the ideal covariance matrix $\mathbf{R}(t)$ (12), which is computed from infinite number of data samples, used in (14) is not available, and has to be replaced by the sample covariance matrix. If the full matrix capture data acquisition is used, the estimate can be obtained by

$$\hat{\mathbf{R}}(t) = \frac{1}{N}\sum_{k=1}^{N} \mathbf{x}^k(t)\,\mathbf{x}^k(t)^H, \tag{15}$$

where $\boldsymbol{x}^k(t)$ is the delayed array output vector when the $k$th array element is excited in transmission and the array is focused on the point of interest in reception.

The minimum variance beamformer is an optimal spatial filter that maximizes the array output signal-to-interference-plus-noise ratio (SINR) [29]. However, its performance degrades in the presence of mismatches or errors like wrong assumptions of acoustic velocity or phase aberrations. This phenomenon is referred to as signal self-nulling, since the mismatches lead to targets appearing slightly out of focus and the beamformer will treat them as interference and try to minimize them [30, 31]. There exist several methods for increasing the robustness at the expense of resolution. Diagonal loading [32] is found to be a straightforward and effective approach in this application, where a constant $\eta$ is added to the diagonal of the estimated covariance matrix

$$\hat{\mathbf{R}}_{DL}(t) = \hat{\mathbf{R}}(t) + \eta\mathbf{I}, \tag{16}$$

where $\mathbf{I}$ is a $N \times N$ identity matrix, and

$$\eta = \frac{1}{N} tr\left[\hat{\mathbf{R}}(t)\right], \tag{17}$$

where $tr[\bullet]$ denotes the trace operator. The amount of diagonal loading in (17) is proportional to the power in the received signals. However, $\eta$ can be tweaked to make a

trade-off between robustness and resolution, and a greater $\eta$ leads to a more robust beamformer in (14), but the resolution is decreased.

## 4. SIMULATION AND EXPERIMENT RESULTS

In this section, we present the simulation and experiment results to evaluate the performances of the adaptive beamformer and the matched filter for interference and noise reduction, against the gold-standard Total Focusing Method (TFM) [2].

### 4.1. Simulation studies

The schematic of a simulated specimen is shown in Fig. 3, where multiple single and paired point reflectors are located at different depths and lateral positions. The material is assumed to be ideal, homogeneous and lossless with the wave propagation speed $c$ = 6,300 m·s$^{-1}$. A 5 MHz linear transducer array is utilized in contact with the specimen upper surface, which consists of 64 omni-directional elements with the inter-element spacing 0.63 mm that is exactly the half wavelength in the medium at the centre frequency of the transducer. The output signal of each element is a five cycle, Gaussian windowed tone burst with a centre frequency of 5 MHz and a −6 dB bandwidth of 50%. The reflectors have a normalized unity amplitude with white Gaussian noise being added to the signals, corresponding to a SNR = 20 dB for a single echo and channel. The sampling rate is 100 MHz.

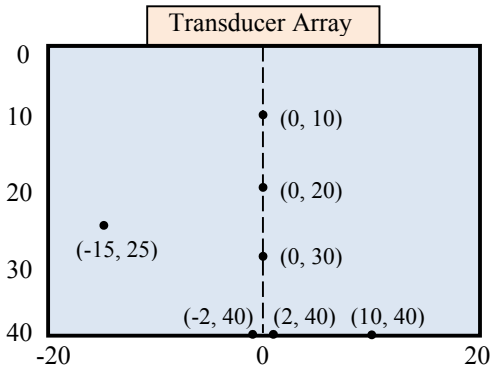


Figure 3. Schematic of simulated sample.

In the simulation studies, the capability of adaptive beamforming to image point reflectors and resolve closely spaced emitters is assessed and compared against that of the delay-and-sum beamformer. Fig. 4 shows the images with a 70 dB dynamic range obtained by using TFM [Fig. 4(a)] and adaptive beamforming in reception [Fig. 4(b)] respectively, and the lateral profiles of the images at the depth of 30 mm are depicted in Fig. 5.

It can be seen in Fig. 4(a), using TFM, the sidelobe indications are pretty visible, especially in the regions close to the main lobe, which potentially hinder the detection of surrounding smaller or weaker reflectors and limit the capability to resolve clustered reflectors. When adaptive beamforming is applied, the image quality is significantly enhanced in terms of clutter noise, image resolution, contrast, and dynamic range as shown in Fig. 4(b). The lateral profiles in Fig. 5 indicate that the main lobe width is more than 50% smaller (−6 dB main lobe width of TFM being 0.93 mm and that of adaptive beamforming being 0.42 mm) and the noise is reduced by more than 30 dB, when adaptive beamforming is applied.

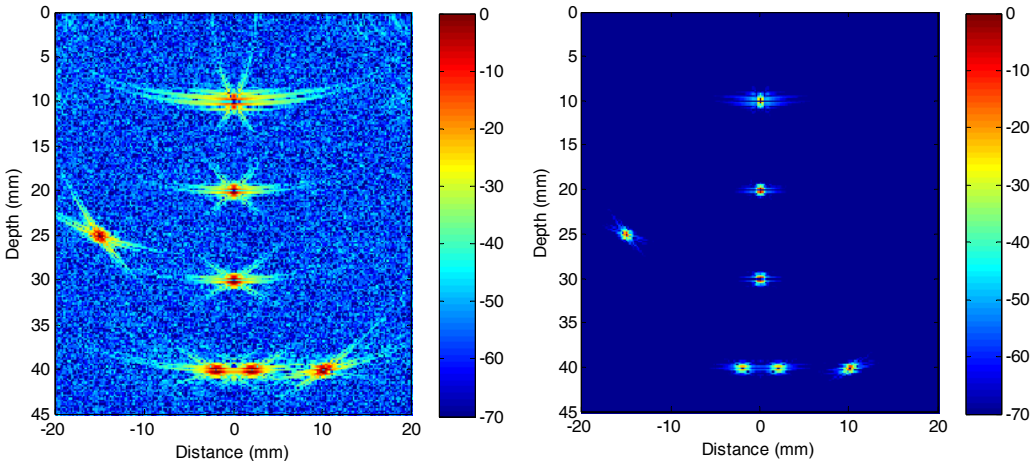


Figure 4. Images of simulated sample. (a) TFM, and (b) Adaptive beamforming.

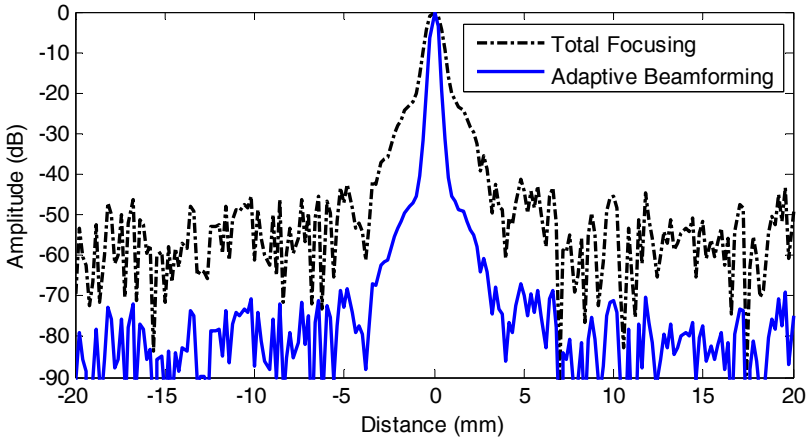


Figure 5. Lateral profiles of images at depth of 30mm.

4.2. Experimental verification

The experimental apparatus consists of three components, namely, test sample, array transducer, phased array control system with a personal computer for excitation and signal processing. A 128-element transducer array with 0.7 mm element pitch and 5 MHz central frequency (Vermon, Tours, France) is utilized in contact with the test sample upper surface with gel coupling, as shown in Fig. 6(a). An OPEN ultrasonic phased array control system with 128 independent parallel channels and 16-bit resolution (LeCouer, Chuelles, France) is connected with the transducer array for excitation and data acquisition, as shown in Fig. 6(b). A personal computer is connected to the OPEN system to control the excitation sequence and record the return signals for post processing and imaging. A MATLAB (The MathWorks, Natick, MA) routine is developed to implement the Full Matrix Capture (FMC) data acquisition, where each transducer element is excited sequentially and the echoes received by all the array elements are recorded [2]. A complete FMC data set is composed of $N^2$ A-scan waveforms, where $N$ is the number of array elements. FMC data are recorded at a sampling rate of 100 MHz, and each A-scan waveform is band-pass filtered to remove the DC drift and high frequency noise.

(a) (b)

Figure 6. Experiment apparatus. (a) Transducer array and test sample, and (b) OPEN phased array control system.

**Table 1. PSO parameters**

| PSO Parameters | Value |
|---|---|
| $K$ | 15 |
| Number of Particles | 150 |
| Number of Iterations | 500 |
| $c_1$ | 0.4 |
| $c_2$ | 1.2 |
| Inertia Weight | 0.8 |

In the experiments, the matched filter response is formulated using equation (5) with $K$ reflectors and all the unknown parameters are captured in a vector with a dimension of $2K \times 1$, consisting of $A_i$ and $t_i$, $i=1, 2, ..., K$. $K$ is pre-determined and set $K=15$, which seems to be not highly sensitive to the performance, provided that a reasonably large $K$ is employed. The PSO paradigm is employed to tackle the problem at hand, because PSO is simple to implement, but it is as powerful as other popular evolutionary algorithms like the Genetic Algorithms, and is robust to the selection of control parameters [28]. The key parameters used in the PSO routine are summarized in Table 1, and the convergence is observed in all the experiments within the maximum number of iterations.

A test sample with a thickness of around 150 mm made of INCONEL Alloy 617 is employed in the experiments. As shown in the datasheet, INCONEL Alloy 617 is a solid-solution, nickel-chromium-cobalt-molybdenum alloy with an exceptional combination of high-temperature strength and oxidation resistance [33]. Alloy 617 is widely used in a variety of key industrial sectors like Energy, Oil and Gas, and Nuclear for components such as ducting and combustion cans. Due to the size of microstructure grain, Alloy 617 is demonstrated to be highly scattering to 5 MHz ultrasound, and results in significant grain noise and pretty low SNR.

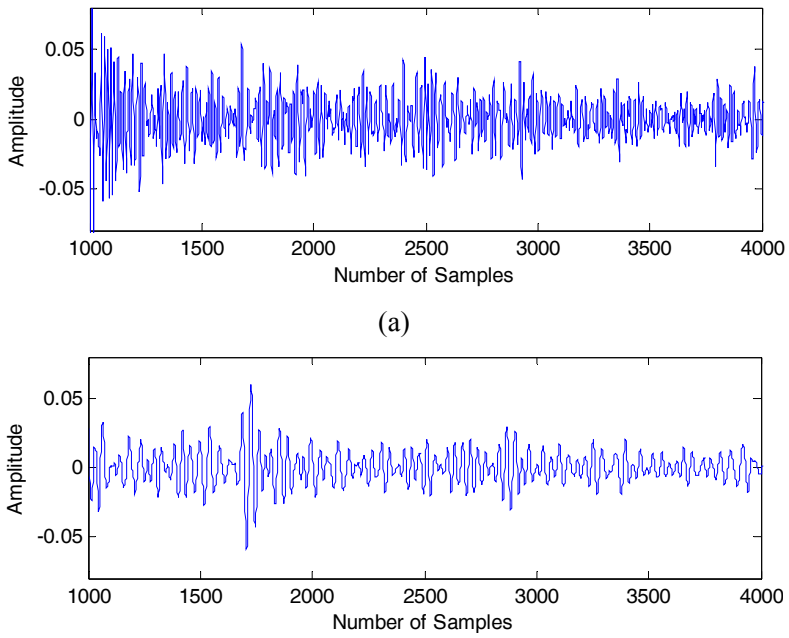


Figure 7. A-scan waveforms at Element 40. (a) Original, and (b) Matched filtered.

Fig. 7(a) shows the A-scan waveform of the echo at Element 40 when the same transducer element is excited, the reflection from a major defect happens around the

samples of 1630-1730. Due to the dominant grain noise, it is almost impossible to identify this reflection, and the SNR is measured to be -9 dB. Fig. 8(a) demonstrates the image obtained with TFM using the original FMC dataset in a dynamic range of 40 dB. The image is pretty noisy and the back-wall is only partially visible at the depth of 147 mm.

Fig. 7(b) illustrates the same echo at Element 40 as in Fig. 7(a), but processed with the optimized matched filter. Comparing to the original signal in Fig. 7(a), it is evident that the defect echo has been enhanced and the grain noise has been suppressed with matched filtering, and it becomes much more confident to detect the defect from thresholding the amplitude. In terms of quantitative comparison, the SNR is increased to 7 dB, and the matched filter observes 16 dB SNR gain for the A-scan signal. To form the image in Fig. 8(b), firstly, each individual A-scan waveform in the FMC data set is matched filtered, and then the processed FMC data set is imaged with TFM. Comparing to the image in Fig. 8(a), it is evident that the clutter noise is greatly reduced, while the back wall reflection is further enhanced.

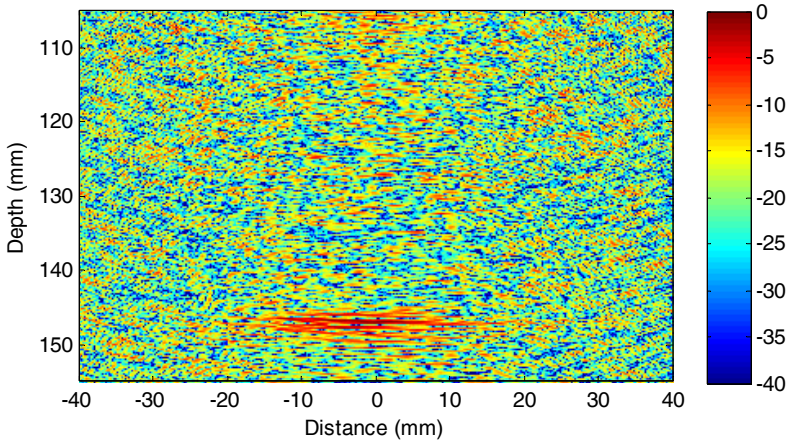


(a)

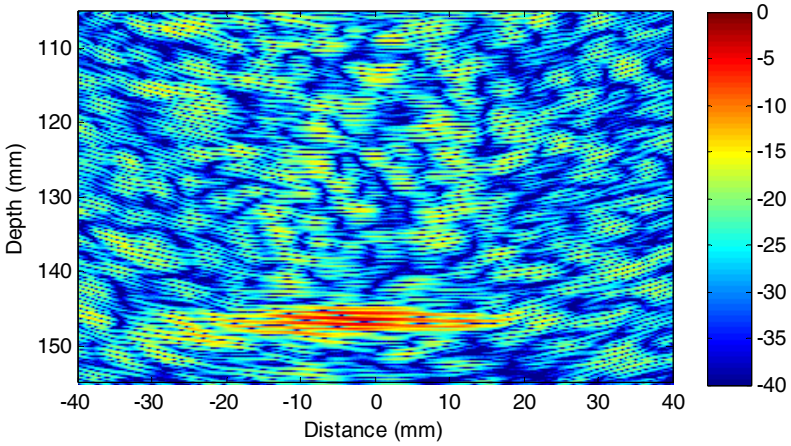


(b)

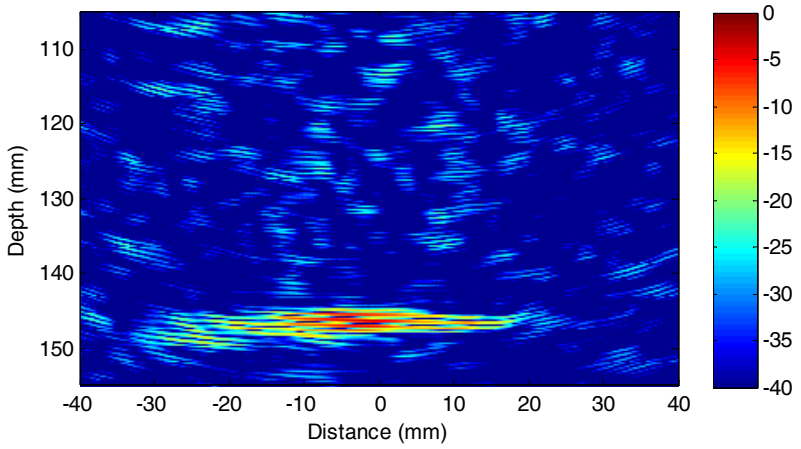


(c)

Figure 8. Images of Alloy 617 test block. (a) TFM with original FMC data, (b) TFM with matched filtered FMC data, and (c) Adaptive beamforming with matched filtered FMC data.

The matched filter works in the temporal-spectral domain, and the adaptive beamformer exploits the spatial diversity along the transducer array aperture. Apparently, there is a potential to combine these two techniques since they work in different domains and may complement with each other for noise reduction. Fig. 8(c) shows the image obtained with the minimum variance beamformer using the matched filtered FMC data set. It is evident that the clutter noise is further reduced, and the back-wall reflection is greatly enhanced in term of the strength as well as the visible lateral length, due to the exploitation of both temporal and spatial characteristics.

## 5. CONCLUSION

This chapter addresses the challenging problem of noise reduction in ultrasonic NDE, and focuses on matched filtering and adaptive beamforming for enhanced SNR and robust defect detection. Matched filtering is demonstrated to be a powerful and effective tool for the problem at hand, and a flexible approach to optimal matched filter design is presented, where the simulated excitation signals are utilised with the control parameters being tweaked and optimized taking into account the actual responses of transducers, the transceiver channels, and the test sample characteristics. The filter is tuned to match the unknown defect echoes instead of the excitation signal, and the response is dependent on the material properties. Minimum variance beamforming demonstrates significant performance improvement over the standard delay-and-sum operation, and diagonal loading further increases its robustness in ultrasonic NDE. With adaptive beamforming applied spatially to the observations across the probe aperture, the spurious echoes and clutter noise are significantly reduced. Simulation studies confirm that the noise level is

reduced by more than 30dB and the resolution is improved twice when adaptive beamforming is employed in the scenario of multiple point reflectors. Experiments on an industrial sample of INCONEL Alloy 617 are conducted and the results verify the advantages and robustness of the approaches when applied separately, and confirm the greater benefits when they are combined to complement with each other as they work in temporal- and spatial- domains respectively. It can be concluded that, the approaches offer a great potential to inspect coarse-grained materials, enhance sensitivity to smaller flaws, increase imaging resolution and contrast, and improve the definition of defect size and shape in NDE.

## REFERENCES


[1] R. B. Thompson and D. O. Thompson, "Ultrasonics in nondestructive evaluation," *Proc. of the IEEE*, vol. 73, pp. 1716-1755, Dec. 1985.

[2] M. Li and G. Hayward, "Ultrasound non-destructive evaluation (NDE) imaging with transducer arrays and adaptive processing," *Sensors,* vol. 12, pp. 42-54, Jan. 2012.

[3] E. P. Papadakis, "Ultrasonic attenuation caused by scattering in poly-crystalline metals," *J. Acoust. Soc. Amer*, vol. 37, pp. 703-710, 1965.

[4] S. P. Neal, P. L. Speckman and M. A. Enright, "Flaw signature estimation in ultrasonic nondestructive evaluation using the Wiener filter with limited prior information," *IEEE Trans. Ultrason., Ferroelect., Freq. Contr.*, vol. 40, pp. 347-353, July 1993.

[5] M. A. G. Izquierdo, M. G. Hernández, O. Graullera and L. G. Ullate, "Time-frequency Wiener filtering for structural noise reduction," *Ultrasonics*, vol. 40, pp. 259-261, May 2002.

[6] I. Amir, N. M. Bilgutay and V. L. Newhouse, "Analysis and comparison of some frequency compounding algorithms for the reduction of ultrasonic clutter," *IEEE Trans. Ultrason. Ferroelectr. Freq. Contr.*, vol. 33, pp. 402-411, 1986.

[7] T. Qi and N. M. Bilgutay, "Statistical analysis of split spectrum processing for multiple target detection," *IEEE Trans. Ultrason., Ferroelect., Freq. Contr.*, vol. 45, pp. 251-256, Jan. 1998.

[8] K. Ho, M. Li, R. O'Leary and A. Gachagan, "Application of frequency compounding to ultrasonic signals for the NDE of concrete," in *Review of Progress in Quantitative Nondestructive Evaluation*, eds. D. O. Thompson and D. E. Chimenti, (American Institute of Physics 1430, Melville, NY), vol. 31, pp. 1508-1515, 2012.

[9] R. Gongzhang, M. Li, T. Lardner and A. Gachagan, "Robust defect detection in ultrasonic nondestructive evaluation (NDE) of difficult materials," *Proc. 2012 IEEE International Ultrasonics Symposium (IUS)*, pp. 467-470, Oct. 2012.

[10] R. Gongzhang, M. Li, B. Xiao, T. Lardner and A. Gachagan, "Robust frequency diversity based algorithm for clutter noise reduction of ultrasonic signals using multiple sub-spectrum phase coherence," in *Review of Progress in Quantitative Nondestructive Evaluation*, eds. D. E. Chimenti, L, J. Bond and D. O. Thompson, (American Institute of Physics 1581, Melville, NY), vol. 33, pp. 1948-1955, 2014.

[11] B. Xiao, M. Li, R. Gongzhang, R. O'Leary and A. Gachagan, "Image de-noising via spectral distribution similarity analysis for ultrasonic non-destructive evaluation," in *Review of Progress in Quantitative Nondestructive Evaluation*, eds. D. E. Chimenti, L, J. Bond and D. O. Thompson, (American Institute of Physics 1581, Melville, NY), vol. 33, pp. 1941-1947, 2014.

[12] M. Li and G. Hayward, "A rapid approach to speckle noise reduction in ultrasonic non-destructive evaluation using matched filters," *Proc. 2014 IEEE International Ultrasonics Symposium (IUS)*, pp. 45-48, Sept. 2014.

[13] M. Li and G. Hayward, "Optimal matched filter design for ultrasonic NDE of coarse grain materials," in *Review of Progress in Quantitative Nondestructive Evaluation*, eds. D. E. Chimenti and L. J. Bond, (American Institute of Physics 1430, Melville, NY), vol. 35, pp. 020011 1-9, 2016.

[14] M. Li, G. Hayward and B. He, "Adaptive array processing for ultrasonic non-destructive evaluation," *Proc. 2011 IEEE International Ultrasonics Symposium (IUS)*, pp. 2029-2032, Oct. 2011.

[15] P.-C. Li and M.-L. Li, "Adaptive imaging using the generalized coherence factor," *IEEE Trans. Ultrason., Ferroelect., Freq. Contr.*, vol. 50, pp. 128-141, Feb. 2003.

[16] T. Lardner, M. Li, R. Gongzhang and A. Gachagan, "A new speckle noise suppression technique using cross-correlation of array subapertures in ultrasonic NDE of coarse grain materials," in *Review of Progress in Quantitative Nondestructive Evaluation*, eds. D. O. Thompson and D. E. Chimenti, (American Institute of Physics 1581, Melville, NY), vol. 32, pp. 865-871, 2013.

[17] T. Lardner, M. Li and A. Gachagan, "Using phase information to enhance speckle noise reduction in the ultrasonic NDE of coarse grain materials," in *Review of Progress in Quantitative Nondestructive Evaluation*, eds. D. E. Chimenti, L, J. Bond and D. O. Thompson, (American Institute of Physics 1581, Melville, NY), vol. 33, pp. 1061-1069, 2014.

[18] D. Gjessing, "Adaptive techniques for radar detection and identification of objects in an ocean environment," *IEEE Journal of Oceanic Engineering*, vol. 6, pp. 5-17, Jan. 1981.

[19] K. Srinivasan, C. P. Chiou and R. B. Thompson, "Ultrasonic flaw detection using signal matching techniques," in *Review of Progress in Quantitative Nondestructive Evaluation*, eds. D. O. Thompson and D. E. Chimenti, (Plenum Press, NY), vol. 14, pp. 711-718, 1995.

[20] N. Ruiz-Reyes, P. Vera-Candeas, J. Curpian-Alonso, R. Mata-Campos and J. C. Cuevas-Martinez, "New matching pursuit-based algorithm for SNR improvement in ultrasonic NDT," *NDT&E International*, vol. 38, pp. 453-458, June 2005.

[21] M. Li and Y. Lu, "Improving the performance of GA-ML DOA estimator with a resampling scheme," *Signal Processing*, vol. 84, pp. 1813-1822, Oct. 2004.

[22] M. Li and Y. Lu, "Source bearing and steering-vector estimation using partially calibrated arrays," *IEEE Trans. Aerosp. Electron. Syst.*, vol. 45, pp. 1361-1372, Oct. 2009.
[23] M. Li and Y. Lu, "Optimal direction finding in unknown noise environments using antenna arrays in wireless sensor networks," *Proc. 7th International Conference on Intelligent Transportation Systems Telecommunications (ITST2007)*, pp. 332-337, June 2007.
[24] M. Li, K. S. Ho and G. Hayward, "Accurate angle-of-arrival measurement using particle swarm optimisation," *Wireless Sensor Network*, vol. 2, pp. 358-364, May 2010.
[25] C. Holmes, B. Drinkwater and P. Wilcox, "Post-processing of the full matrix of ultrasonic transmit-receive array data for non-destructive evaluation," *NDT&E International*, vol. 38, pp. 701-711, Aug. 2005.
[26] R. Eberhart and J. Kennedy, "A new optimizer using particle swarm theory," *Proc. 6th International Symposium on Micro Machine and Human Science*, pp.39-43, Oct. 1995.
[27] M. Li and Y. Lu, "A refined genetic algorithm for accurate and reliable DOA estimation with a sensor array," *Wireless Personal Communications*, vol. 43, pp. 533-547, Oct. 2007.
[28] M. Li and Y. Lu, "Maximum likelihood DOA estimation in unknown colored noise fields," *IEEE Trans. Aerosp. Electron. Syst.*, vol. 44, pp. 1079-1090, Jul. 2008.
[29] J. Capon, "High-resolution frequency-wavenumber spectrum analysis," *Proc. of the IEEE*, vol. 57, pp. 1408-1418, 1969.
[30] J. F. Synnevag, A. Austeng and S. Holm, "Adaptive beamforming applied to medical ultrasound imaging," *IEEE Trans. Ultrason. Ferroelectr. Freq. Contr.*, vol. 54, pp. 1606-1613, Aug. 2007.
[31] M. Li and Y. Lu, "Dimension reduction for array processing with robust interference cancellation," *IEEE Trans. Aerosp. Electron. Syst.*, vol. 42, pp. 103-112, Jan. 2006.
[32] J. Li, P. Stoica and Z. Wang, "On robust Capon beamforming and diagonal loading," *IEEE Trans. Sign. Process.*, vol. 51, pp. 1702-1715, 2003.
[33] INCONEL 617 Technical Data, http://www.hightempmetals.com/techdata/hitempInconel617data.php, accessed in February 2018.